Elastic and Thermal Properties of Hexagonal Perovskites

A. Chernatynskiy[1,2], A. Auguste[1†], B. Steele[1††], J. E. Phillpot[1†††], R. W. Grimes[3], and S. R. Phillpot[1]*

[1] Department of Materials Science and Engineering, University of Florida, Gainesville FL 32611

[2] Department of Physics, Missouri University of Science and Technology, Rolla MO 65401

[3] Department of Materials, Imperial College London, SW7 2AZ, United Kingdom

Abstract

We systematically investigate the mechanical and thermal properties of the $P6_3cm$ hexagonal perovskites with composition $A^{3+}B^{3+}O_3$ for potential use in thermal barrier coatings. In spite of the structural anisotropy, the elastic constants are essentially isotropic. The thermal expansion is, however, strongly anisotropic, while the thermal conductivity is relatively isotropic. The thermal conductivities of the hexagonal perovskites are much larger than those of the orthorhombic perovskites.

To be submitted to the Computational Materials Science

† Current address: Department of Polymer Science and Engineering, University of Massachusetts, Amherst MA 01003

†† Current Address: CEMEX, Brooksville FL 34601

††† Current Address: Google, Kirkland WA 98033

* Corresponding author: sphil@mse.ufl.edu

1. Introduction

Materials with high melting temperatures and low thermal conductivities have numerous applications, including thermal barrier coatings (TBCs). Currently, yttria-stabilized zirconia (YSZ) is the ceramic most commonly used for such applications due to its durability and stability at high temperatures. However, there is still a need to improve the performance of TBCs, one aspect of which is identifying materials with low or exploitable thermal-transport properties.[1] Low thermal conductivity is, though, not the only criterion by which a TBC material is selected: other important factors include mechanical and chemical stability. One of the crucial elements of the former is that thermal expansion of the coating has to match that of the underlying material. For example, when a TBC is applied to a turbine blade, the thermal expansion of the TBC ought to match that of the nickel superalloy which forms the body of the blade.

Candidate materials to replace YSZ are expected to be found among oxides with more complex structures.[2] For example, other fluorite-related structures such as the pyrochlores offer thermal conductivities as low as YSZ.[3] Also of interest are perovskites and related materials.[4] As a general strategy, exploring structural anisotropy may be a useful tool for the development of optimally low thermal conductivity materials. In a previous paper[5] we studied in detail the relationship between the structure, elastic properties, thermal expansion and thermal conductivity for a series of orthorhombic $A^{3+}B^{3+}O_3$ perovskites; various choices of A and B give lesser or greater departures from the ideal cation radii ratio[6] and therefore display structures with varying degrees of anisotropy. A similar study of some of the structural and elastic properties was made on a smaller subset of these orthorhombic perovskites.[7] The simulation results showed that the structure and thermal transport properties are related to the degree of tilting of the BO_6 octahedra and to the size of the A and B ions. Weak anisotropy in the structure manifested itself in direction-dependent thermal properties.

The orthorhombic structure becomes unstable if the cation radii ratio deviates too much from the ideal value. For even larger deviations, the $A^{3+}B^{3+}O_3$ perovskites crystallize into an anisotropic hexagonal structure. The purpose of this paper is to characterize the thermal properties of $A^{3+}B^{3+}O_3$ perovskites in the hexagonal structure using atomic-level simulation methods. Comparison to the orthorhombic *Pbnm* structured perovskites will allow us to gain a better insight as to how the cation radius ratio affects the structure and properties of hexagonal perovskites.

2. Structure and composition

The $A^{3+}B^{3+}O_3$ perovskites form a large family. Here, we focus on A = Sc, In, Lu, Yb, Er, Ho, Y, Dy, Tb, Gd, Eu, Sm, Nd, Pr, Cr, and La, combined with B = In, Sc, Fe, Ga, Cr, and Al. Depending on the radii of the specific elements involved, these perovskites crystallize into the orthorhombic *Pbnm,* hexagonal $P6_3/mmc$ or lower symmetry $P6_3cm$, hexagonal $R\bar{3}c$ and bixbyite *Ia3* structures, as illustrated in Figure **1**.[5, 8]

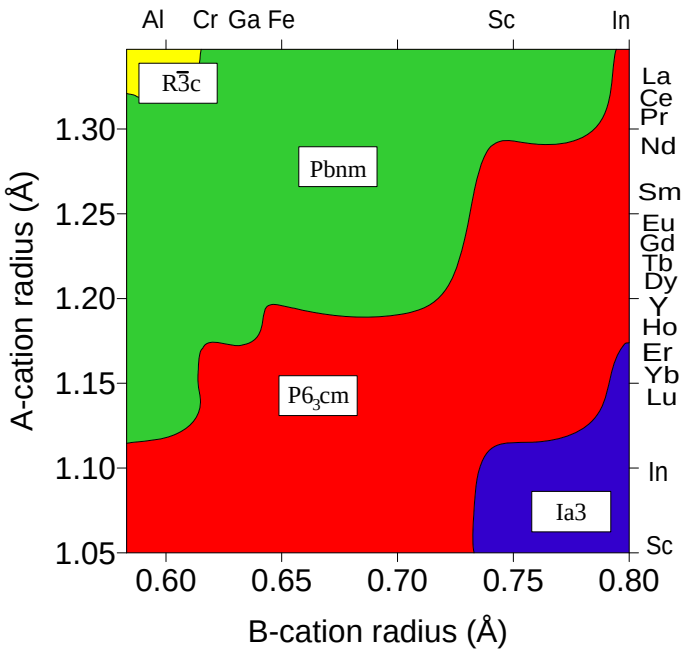

Figure 1. Stability map for structures of various A-B combinations within $A^{3+}B^{3+}O_3$ perovskite materials [5, 8]. The blue region corresponds to the region of stability of the bixbyite *Ia3* structure; the red corresponds to the hexagonal *P6₃cm* structure; the green region corresponds to the orthorhombic *Pbnm* structure; the yellow region corresponds to the hexagonal $\boldsymbol{R\bar{3}c}$ structure.

The differences in the perovskite crystal structure displayed can be understood in terms of the ionic radii of the cations involved. In order to characterize this size effect, the tolerance factor, τ, was introduced[6] for this structure:

$$\tau = \frac{R_A + R_O}{\sqrt{2}\left(R_B + R_O\right)} \tag{1}$$

If the ionic radii of the cations A and B are such that τ is equal to unity then the ideal cubic perovskite ($Pm\bar{3}m$) is expected to form; if τ deviates from unity, one expects distortions in the structure.

For small deviations (τ ~ 0.9-1.0) distortions in the structure lead to the formation of orthorhombic perovskites,[5, 9] while for larger deviations the structure changes completely to hexagonal, as indicated in Figure 2. First principles calculations and experiments[10] on the $AGaO_3$ and $AInO_3$ families agree that at low temperature the structure belongs to $P6_3cm$ symmetry group, while at elevated temperatures above ~1500K it transitions to the higher symmetry $P6_3/mmc$ group. The lower symmetry structure differs by the slight tilting of the bipyramids and corrugation of the A-cation layer along the z-direction. Interatomic potentials utilized in this work appear to stabilize the hexagonal structure in $P6_3/mmc$ symmetry at all temperatures. This is in contrast to previous reports;[5, 8] however due to very slight variations in the structures the difference can easily be overlooked. Since we are interested in high-temperature behavior of these compounds and high symmetry structure features anisotropic behavior due to the layered

discussed below, the $P6_3/mmc$ is more relevant and we need not be concerned with the small differences between these crystal structures.

The hexagonal perovskite structure is not a classic perovskite but rather an intermediate structure between the bixbyite and perovskite structures. In particular, the B ions and oxygen ions form triangular bipyramids. We will denote the oxygen atoms that are in the same plane with B-cations as in-plane oxygens (O_P), while those that form their own separate planes are denoted as on-top oxygens (O_T).

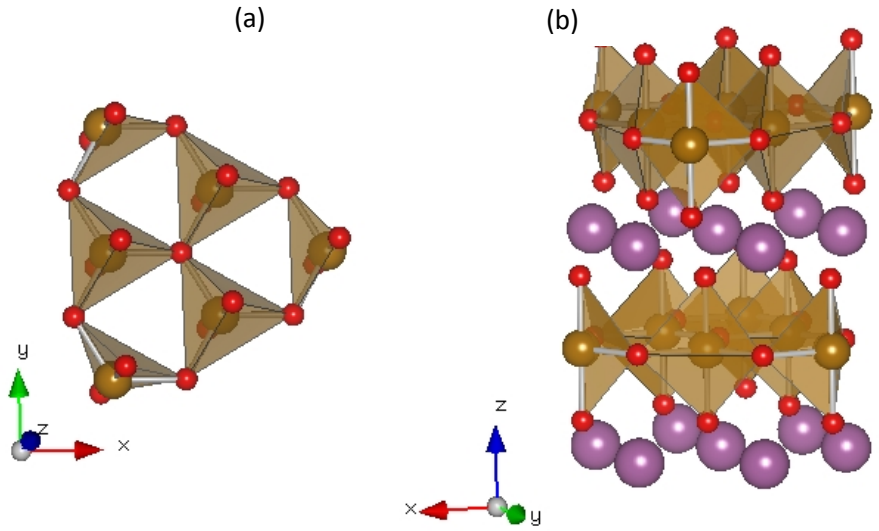

Figure 2. The *P6₃cm* hexagonal perovskite structure from different perspectives: (a) along the z-axis, parallel to [0001] (b) in the x-y plane. The oxygen ions are red, A cations are purple, B cations are brown.

These polyhedra form a corner-sharing honeycomb lattice in the x-y plane, as illustrated in Figure 2(a). Figure 2(b), shows that the A ions are located above the corner edges of the bipyramids in a separate plane. Thus the polyhedra are not connected in the [0001] direction; as we shall see, this has profound effects on the properties of these materials. Analyzing the bond lengths in the hexagonal perovskites one observes that both A-O_T (2.1-2.3 Å) and B-$O_{P,T}$ (1.9-2.1 Å) bonds have similar values, contrary to the case of the orthorhombic perovskites, where the A-O bonds is of the order of 2.6-2.8 Å. We attribute that significant shortening of the A-O_T bond to the enhancement of the electrostatic interactions between oxygens and A-cations in the hexagonal structure. Subsequent layers of the A-cations, on-top oxygens O_T, B-cations and O_T's have formal charges of +3 : -2 : +1 : -2, respectively. Therefore, the electrostatic interaction between an A-cation layer and an O_T layer is much stronger then between a B-cation layer and O_T. It is, in fact, more appropriate to think of O_T's forming prismatic polyhedra around A-cations. Despite this layering, these materials are quite dissimilar to 2D materials such as graphite, in which interlayer bonds are of the van der Waals type, and are significantly weaker than intralayer covalent bonds, while in the hexagonal perovskites all bonds are ionic/covalent.

The hexagonal symmetry of the crystal dictates the symmetry of the tensors that represent its physical properties. In particular, all second rank tensors (which include the thermal expansion and thermal conductivity) are isotropic in the x-y plane but have a different value along the z-direction with off-diagonal components equal to zero.[11] Thus, the thermal conductivity can be characterized by two

constants: k_{11} and k_{33}. The elastic properties are described by 6 independent elastic constants: C_{11}, C_{33}, C_{12}, C_{13}, C_{44} and C_{66}.

The stability diagram in Figure 1, which was determined from atomic-level simulations, using the same empirical interatomic potentials as used in this study, it is in general agreement with experiment and DFT calculations.[10] However, X-ray diffraction studies of $HoFeO_3$ concluded that it was an orthorhombic perovskites,[12] rather than hexagonal as predicted by the simulations; for this specific composition, the behavior did not follow those of other related materials: $LaFeO_3$, $SmFeO_3$, $PrFeO_3$, and $GdFeO_3$, pointing to the somewhat anomalous behavior of this material.

3. Simulation methods

Structural parameters and elastic constants are determined by the lattice-statics method, as implemented in the General Utility Lattice Program (GULP).[13, 14] The long-range interatomic interactions are taken into account by Coulombic interactions while the short-ranged interactions are described by the Buckingham potential:

$$V(r_{ij}) = Ae^{-r_{ij}/\sigma} - \frac{B}{r_{ij}^6} \quad (2)$$

In Eq. 2, r_{ij} is the distance between ions *i* and *j*, while *A, B* and *σ* are parameters specific to each ion pair. Parameters from Levy *et al.* are used for the short-ranged interactions.[8] The thermal expansion is determined within the quasi-harmonic approximation.[15]

The thermal conductivities of representative systems are calculated using a Boltzmann Transport Equation (BTE) approach, as implemented in the PhonTS computational package. [16, 17] Compounds in this family are electrical insulators, and thus lattice thermal transport is the dominant mechanism. We choose to examine 16 systems: 8 of them are hexagonal perovskites ($AFeO_3$, A=Ho, Er, Yb, Lu, In and Sc and $HoBO_3$, B=Fe, Sc and In), while 8 are orthorhombic with the same cations ($AFeO_3$, A=Ce, Sm, Gd and Dy and $HoBO_3$, B=Al, Cr and Ga). The systems examined are selected so that the contributions to the thermal conductivity of the A and B ions can be determined separately. Orthorhombic perovskite are included in order to consistently explore the effect of the phase boundary between hexagonal and orthorhombic perovskites on thermal transport. In each case, the simulated unit cell is an orthorhombic cell with 20 atoms. For orthorhombic perovskites, we employed k-mesh of 9x9x9, while for hexagonal perovskites the k-mesh is 13x9x7. Denser k-points results in variation of thermal conductivity within 3% of the presented results. BTE calculations produce the entire thermal conductivity tensor, thereby enabling us to explore the anisotropy in thermal transport properties.[5, 18, 19] This method of calculation of the thermal conductivity is not the same as that used in the earlier analysis of the orthorhombic structures, which used direct molecular-dynamics simulation. For the orthorhombic systems that were analyzed previously and revisited here, the results from the two methods are very similar but not exactly the same; the small differences do not affect our analyses.

Phonons calculations for the thermal expansion are performed with a 3x3x3 k-mesh; Grüneisen parameters are determined by the numerical differentiation of the phonon frequencies with respect to appropriate strains.

4. Results

Structural Analysis

Figure **3** shows contour plots of the primitive cell volume, as well as lattice constants *a* and *c* as a function of the compositions for the hexagonal perovskites, as obtained from GULP. Unlike the orthorhombic perovskites, the hexagonal *P6$_3$/mmc* system does not involve tilting of the oxygen polyhedra as the composition changes. As a result, all three structural properties increase proportionally to the increase of ionic radii of both A and B cations (i.e., from bottom left to top right). The A-Cation radius affects the lattice constant in the x-y plane somewhat more strongly than along z-direction, which is a result of the stronger electrostatic interactions between A-cation layer and O_T layer: an increase in the A-cation size should push the O_T layer further away from A-cation layer, but strong electrostatic interaction compensates by expanding the lattice in the x-y plane. This is corroborated by the observation that the B-O_P bond length is greater than the B-O_T bond and increases proportionally to the A-cation radius for a fixed B-cation radius.

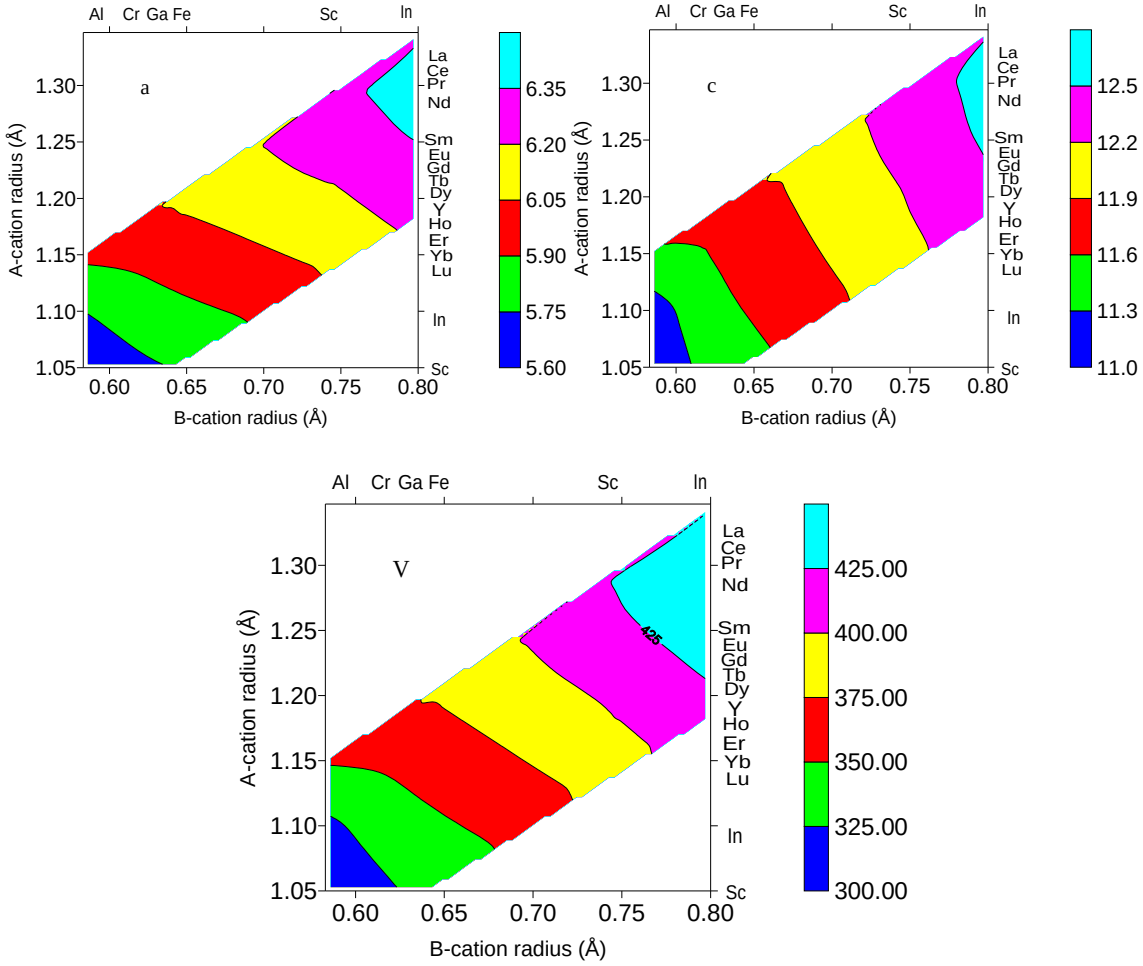

Figure 3. Lattice parameters *a* and *c*, and volume, V(A^3), of the unit cell as a function of composition.

Elastic properties

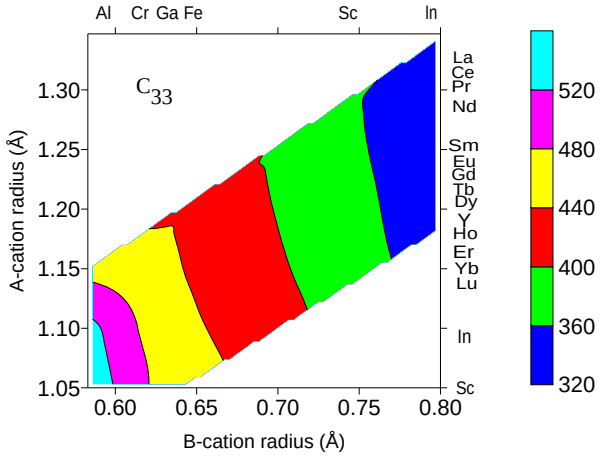

As shown in Figure **4**, the material becomes elastically softer as the A and B cations increase in size. This is directly related to the volume increase of the system shown in Figure 3. The A-cation size and the B-cation size have similar effect on C_{11} and C_{66}, while C_{13}, C_{33} and C_{44} are more dependent on the B-ion. By contrast, C_{12} is essentially independent of the B-ion ionic radius. In the case of the orthorhombic perovskites, the stronger dependence of the elastic constants on the B-cation radius was linked to the largely covalent character of the B-O bond, as opposed to the largely ionic character of the A-O bonding. For the hexagonal perovskites, the strong dependence of C_{12} on the A-cation radius, coupled with the fact that elastic constant in the direction perpendicular to the x-y plane (C_{33}) is higher than the elastic constant parallel to it (C_{11}), lead us to conclude that in hexagonal perovskites the A-O and B-O bonds have similar strength. As mentioned above, the A-O bond length in the hexagonal perovskites is about 2.1-2.3 Å and comparable in length to B-O bond length is 1.9-2.1 A, which also supports this conclusion.

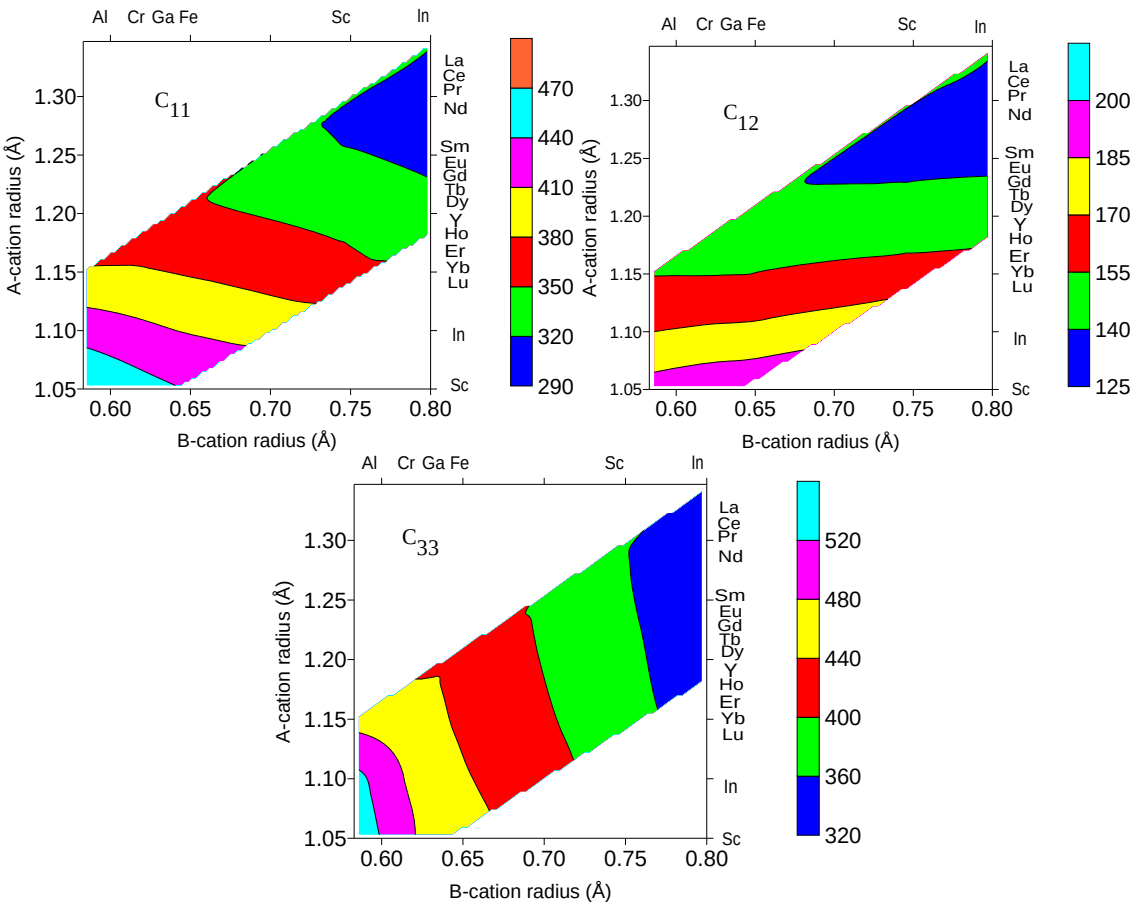

Figure 4. Representative elastic constants calculated by GULP for the hexagonal *P6₃cm* structured perovskites

Thermal expansion

Figure 5 reports predicted thermal expansion coefficients, calculated within the quasi-harmonic approximation. This suggest that the *P6₃cm* perovskites exhibit strongly anisotropic thermal expansion coefficients with α_{11} being almost three times larger than α_{33}. This large difference can be attributed to the anisotropic structure. In particular, the lack of connectivity of the polyhedra along the c axis enables the system to expand very easily in this direction. Moreover, α_{33} decreases with decreasing B-cation radius and increasing A-cation radius, while α_{11} shows the opposite trend. Nevertheless, the thermal expansion of hexagonal perovskites in the x-y plane have similar values to those of *Pbnm* perovskites.

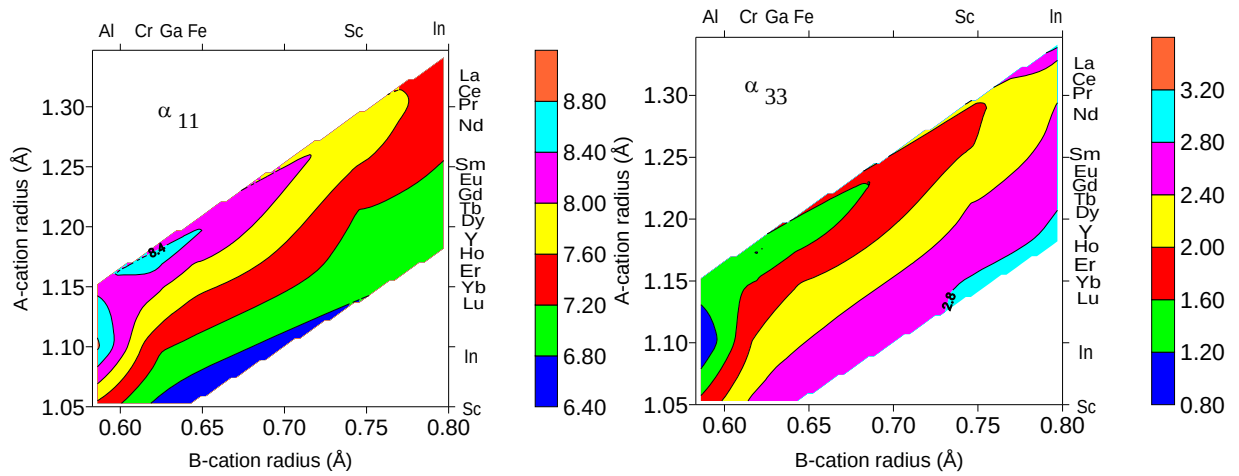

Figure 5. Thermal expansion coefficient (in 10^{-6} K^{-1}) in (a) the a-b plane, and (b) along the c axis. Note the difference in scales

Anisotropy in the thermal expansion or the thermal conductivity of compounds with hexagonal structures is very common. The explanation of such anisotropy typically relies on an analysis of the phonon states in the quasi-harmonic approximation. As shown by Abdullaev**Error! Reference source not found.**, the thermal expansion along the 6-fold axis (α_{33} in our notation) and perpendicular to it (α_{11}) can be expressed as (if λ is an index for the phonon states, combining the reciprocal vector in the Brillouin zone and phonon branch index):

$$\alpha_{11} = \frac{1}{V}\frac{1}{(C_{11}+C_{12})C_{33}-2C_{13}^2}\left(C_{33}\sum_\lambda C_v^\lambda \gamma_x^\lambda - C_{13}\sum_\lambda C_v^\lambda \gamma_z^\lambda\right) \quad (3)$$

$$\alpha_{33} = \frac{1}{V}\frac{1}{(C_{11}+C_{12})C_{33}-2C_{13}^2}\left((C_{11}+C_{12})\sum_\lambda C_v^\lambda \gamma_z^\lambda - 2C_{13}\sum_\lambda C_v^\lambda \gamma_x^\lambda\right) \quad (4)$$

where γ_x and γ_z are the mode-dependent Grüneisen parameters with respect to strains in the x-y plane and along the z direction, C_v is the phonon mode specific heat, and V is the volume of the unit cell. Interplay between mode-specific Grüneisen parameters and elastic constants can produce very strong anisotropy. To take the most extreme example, the thermal expansion in graphite in the z-directions is 12-times the value in the x-y plane. The origin of this anisotropy lies in the weak van der Waals interactions between the covalently bonded graphite layers. In such layered materials transverse acoustic modes have a negative γ_x that is a result of the so called membrane effect[20]: if the interlayer interactions are weak then each layer can be considered a membrane and its transverse modes will have higher frequencies when subject to uniaxial strain. Negative Grüneisen parameters will drive thermal expansion anisotropy.[20]

In the case of the hexagonal perovskites, there are some states that manifest a negative in-plane Grüneisen parameter, but there are very few of them, and they do not contribute significantly to the total thermal expansion. Overall, the membrane effect is not very strong, which is a consequence of the complicated structure of the layers. Instead, there is a group of phonon states in the 8-12 THz range that have a very large in-plane Grüneisen parameter, but a relatively small Grüneisen parameter in the z-direction. Correspondingly, these modes contribute significantly to thermal expansion in the x-y plane but

to thermal contraction in the z-direction. The origin of this strong asymmetry can be understood from an analysis of these phonon states; this analysis reveals that these eigenvectors are dominated by the in-plane motion of the cations, with very little oxygen involvement. Their frequency, therefore, is only weakly affected by the strain in the z-direction (small γ_z), but strongly dependent on the strain in the x-y plane (large γ_x). As a result, these phonon states have a large positive contribution to the thermal expansion in the plane, but a negative contribution to the thermal expansion along z-direction, as illustrated in Figure **6** for the example of the $YbCrO_3$.

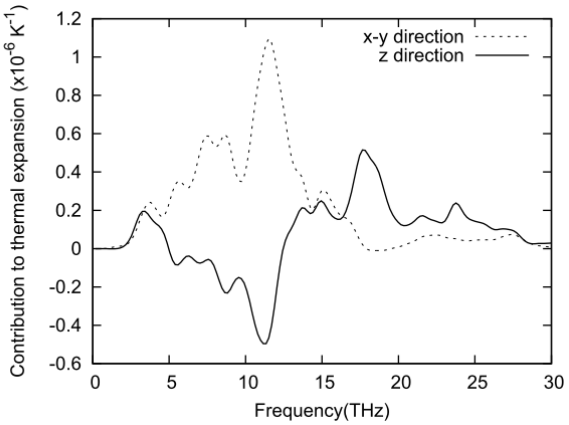

Figure 6. Frequency dependent contribution to thermal expansion along different directions in $YbCrO_3$.

This result can also be quite easily understood from the perspective of the close packing of the atoms in the system: in the x-y plane, A-cations are close packed, while that is not the case along z-direction. As a result, as temperature increases and atoms are displaced further from their equilibrium positions, atoms in plane interact strongly with each other, leading to larger thermal expansion coefficients.

Thermal Conductivity

To examine both the thermal conductivity of the hexagonal phase and to compare with the orthorhombic phase, we have determined the anisotropic thermal conductivity for two cuts across the composition map in Fig. 1: the $AFeO_3$ and $HoBO_3$ series, where A and B are various A-site and B-site cations.

The previous study of the orthorhombic phases found that thermal conductivity was only weakly dependent on the A-cation radius, but seems to increase close to the stability boundary between the orthorhombic and hexagonal phases. Figure 7(a) is consistent with this, showing that orthorhombic $DyFeO_3$, closest to the stability boundary, has the highest thermal conductivity. Most remarkable in Figs. 7(a) and 7(b) is that the hexagonal $AFeO_3$ perovskites display a much higher thermal conductivity than their orthorhombic counterparts.

Figure 7 shows that the anisotropy in the thermal conductivity is generally weak. As discussed above, the A-O and B-O bonds are similar in length, reflecting rather similar bond strengths; Fig. 1 shows, the A-O bonds are primarily along the z-axis, while the B-O bonds are primarily in the xy-plane. These rather equal bond strengths then lead to rather isotropic thermal conductivities. Remarkably however, three

materials $InFeO_3$, $HoScO_3$ and $HoInO_3$ shower a significantly larger thermal conductivity in the z-direction than in the x-y plane. This is opposite to our experience with layered systems in which the weak coupling between layers leads to a lower thermal conductivity on the z direction. This shows that from the thermal perspective, these systems cannot be considered as layered. This apparent discrepancy can be understood in terms of the differing contributions of various phonons to the thermal expansion and conductivity. While phonons with energies greater than ~8 THz do not contribute significantly to the thermal conductivity, they do contribute to the thermal expansion. Moreover, anharmonicity contributes to each in different ways. The thermal expansion depends linearly on the frequency dependent Grüneisen parameter, while the thermal conductivity depends on the square of the Grüneisen parameter.[21,22]

To more clearly identify the effects of crystallography, we determined the thermal conductivity of $HoGaO_3$ in both the orthorhombic and hexagonal structures; although the orthorhombic structure has the lower energy, the hexagonal structure is metastable allowing the determination of its thermal transport properties. As Fig. 8(a) shows, the density of states for the orthorhombic phase shows significantly stronger peaks than that of the hexagonal phase; however, they do span approximately the same frequency range. Fig. 8(b) shows the contribution of phonons in specific frequency ranges (open symbols) and the cumulative contribution (solid symbols). It is evident that the frequencies above 10 THz contribute essentially the same amount for both structures. The big difference comes at lower frequencies, for which these phonons contribute significantly more in the hexagonal structure than in the orthorhombic.

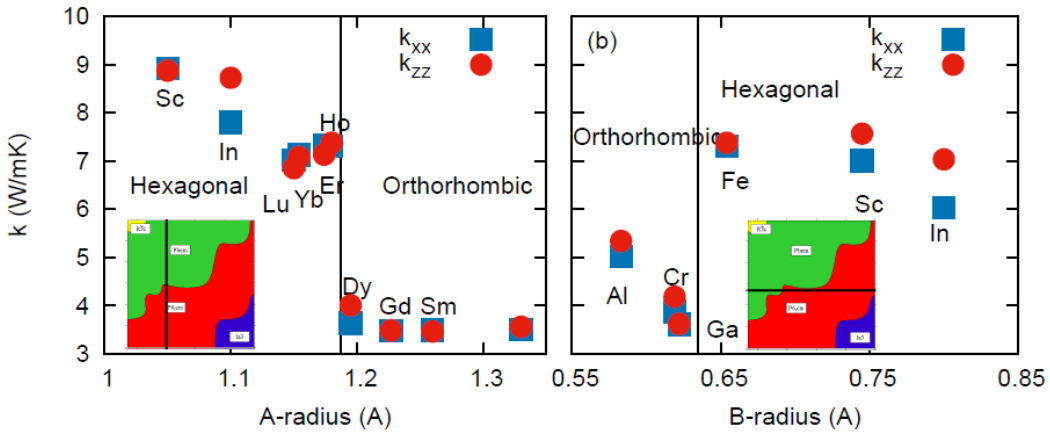

Figure 7. Thermal conductivity of (a) $AFeO_3$ and (b) $HoBO_3$ systems. Vertical line indicates the boundary between hexagonal and orthorhombic structures. Inserts indicate the location of the systems on the diagram from Fig. 1

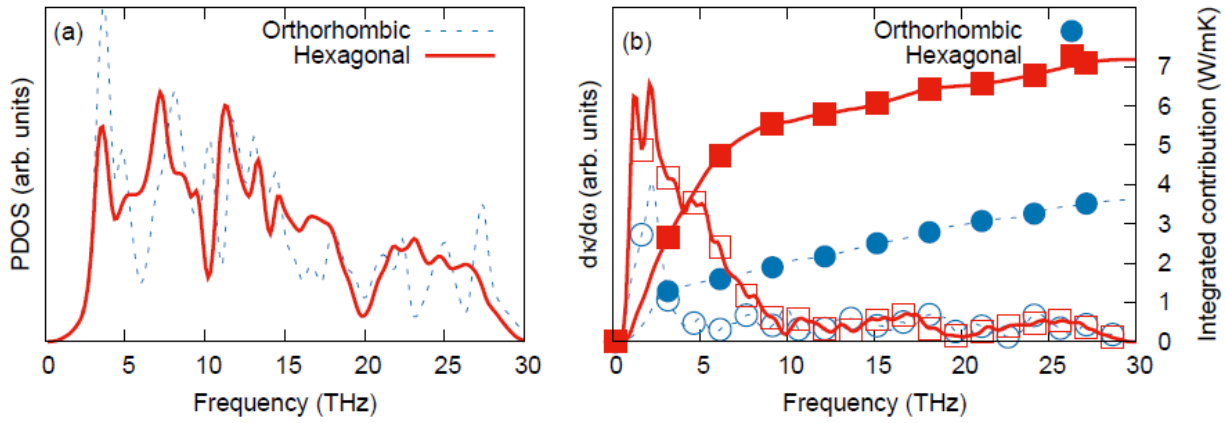

Figure 8. Comparison between hexagonal (red solid lines) and orthorhombic (blue dashed lines) structures in $HoGaO_3$ system: (a) phonon density of states and (b) differential thermal conductivity (open symbols, left axis) and thermal conductivity accumulations function (filled symbols, right axis).

5. Discussion and Conclusions

The mechanical and thermal properties of *P6₃cm* hexagonal perovskites have been investigated using atomic scale computer simulation. The results from the thermal expansion and thermal conductivity simulations illustrate strongly anisotropic behavior in the former case, and weak anisotropy in the latter, indicating the very different roles that anharmonicity play in these two properties. Combined with the previous published simulation results for orthorhombic perovskites, this study shows that the thermal conductivity is significantly larger in the hexagonal structure than in the orthorhombic structure.

Unfortunately, there is no experimental thermal expansion or thermal conductivity data on the hexagonal perovskites considered. The closest system is the multiferroic isostructural compound $YMnO_3$. Its thermal properties do seem to be consistent with those of the systems considered here. In particular, its low-temperature thermal expansion is strongly anisotropic, α_{11} = 9.5 and α_{33}= -6.9 10^{-5} K^{-1}.[23] As can be seen by comparing with Fig. 5, this displays an even stronger anisotropy that that of the system discussed here. By contrast its thermal conductivity shows much less anisotropy: k_{xx}~5.1 and k_{zz}~7.5 W/mK. [24] Of course, that $YMnO_3$ is not a direct analog of the systems considered here as it exhibits much richer ferroelectric and magnetic behavior not considered here.

One motivation for the analysis of the thermal properties of these systems is their potential application as thermal barrier coatings. We have seen that the thermal conductivities of these hexagonal systems are actually quite large compared to that of the ubiquitous stabilized zirconia systems. However, considering these hexagonal perovskites and the previously studies orthorhombic perovskites as a system, they do offer a very rich composition space and two competing structures, which have the potential to be engineered for superior thermal performance.

Acknowledgments

We are grateful for valuable discussions with Susan Sinnott and David R. Clarke. This work was supported by a Materials World Network Project, NSF DMR-0710523. The work of AC was supported by DARPA.

References

[1] D. R. Clarke and S. R. Phillpot, “Thermal barrier coating materials,” *Mat. Today*, vol. 8, pp. 22 – 29, 2005.

[2] W. Pan, S. R. Phillpot, C. Wan, A. Chernatynskiy, and Z. Qu, “Low thermal conductivity oxides,” *MRS Bulletin*, vol. 37, pp. 917–922, 2012.

[3] P. K. Schelling, S. R. Phillpot, and R. W. Grimes, “Optimum pyrochlore compositions for low thermal conductivity,” *Philos. Mag. Lett.*, vol. 84, pp. 127–137, 2004.

[4] R. Mitchell, *Perovskites: Modern and Ancient*. Almaz Press, 2002.

[5] B. Steele, A. D. Burns, A. Chernatynskiy, R. W. Grimes, and S. R. Phillpot, “Anisotropic thermal properties in orthorhombic perovskites,” *J. Mater. Sci.*, vol. 45, pp. 168–176, 2010.

[6] H. D. Megaw, “Crystal structure of double oxides of the perovskite type,” *Proc . Phys. Soc.*, vol. 58, p. 133, 1946.

[7] A. Senyshyn, H. Ehrenberg, L. Vasylechko, J. D. Gale, and U. Bismayer, “Computational study of $LnGao_3$ (Ln = La-Gd) perovskites,” *J. Phys.: Condens. Matter*, vol. 17, p. 6217, 2005.

[8] M. R. Levy, R. W. Grimes, and K. E. Sickafus, “Disorder processes in a3+b3+o3 compounds: implications for radiation tolerance,” *Philos. Mag.*, vol. 84, pp. 533–545, 2004.

[9] A. M. Glazer, “The classification of tilted octahedra in perovskites,” *Acta Cryst. B*, vol. 28, pp. 3384–3392, 1972.

[10] T. Tohei, H. Moriwake, H. Murata, A. Kuwabara, R. Hashimoto, T. Yamamoto, and I. Tanaka, “Geometric ferroelectricity in rare-earth compounds $RGaO_3$ and $RIno_3$,” *Phys. Rev. B*, vol. 79, p. 144125, 2009.

[11] J. Nye, *Physical Properties of Crystals: Their Representation by Tensors and Matrices*. Oxford science publications, Clarendon Press, 1985.

[12] A. Berenov, E. Angeles, J. Rossiny, E. Raj, J. Kilner, and A. Atkinson, “Structure and transport in rare-earth ferrates,” *Solid State Ionics*, vol. 179, pp. 1090 – 1093, 2008. Solid State Ionics 16: Proceedings of the 16th International Conference on Solid State Ionics (SSI-16), Part I.

[13] J. D. Gale, “GULP: A computer program for the symmetry-adapted simulation of solids,” *J. Chem. Soc., Faraday Trans.*, vol. 93, pp. 629–637, 1997.

[14] J. D. Gale and A. L. Rohl, “The general utility lattice program (gulp),” *Mol. Simul.*, vol. 29, pp. 291–341, 2003.

[15] B. Fultz, “Vibrational thermodynamics of materials,” *Prog. Mater. Sci.*, vol. 55, pp. 247–352, 2010.

[16] A. Chernatynskiy and S. R. Phillpot, “Evaluation of computational techniques for solving the Boltzmann Transport Equation for lattice thermal conductivity calculations,” *Phys. Rev. B*, vol. 82, 2010.

[17] A. Chernatynskiy and S. R. Phillpot, “Phonon transport simulator (PhonTS),” *Comp. Phys. Comm.*, vol. 192, pp. 196–204, 2015.

[18] P. K. Schelling, S. R. Phillpot, and P. Keblinski, “Comparison of atomic-level simulation methods for computing thermal conductivity,” *Phys. Rev. B*, vol. 65, p. 144306, 2002.

[19] Y. Yang, X. Liu, and J. Yang, “Nonequilibrium molecular dynamics simulation for size effects on thermal conductivity of Si nanostructures,” *Mol. Simul.*, vol. 34, pp. 51–56, 2008.

[20] N. Abdullaev, “Grüneisen parameters for layered crystals,” *Phys. Solid State*, vol. 43, pp. 727–731, 2001.

[21] P.G. Klemens, “Thermal Conductivity and Lattice Vibrational Modes”, *Solid State Physics*, vol. 7, pp. 1-98 (1958).

[22] T. Watanabe, S. B. Sinnott, J. S. Tulenko, R. W. Grimes, P. K. Schelling and S. R. Phillpot, “Thermal transport properties of uranium dioxide by molecular dynamics simulation”, *Journal of Nuclear Materials*, vol. 375, 388-296 (2008).

[23] M. Tomczyk, A. M. Senos, P. M. Vilarinho and I. M. Reaney, “Origin of microcracking in YMnO3 ceramics”, Scripta Materialia, vo. 66, 288-291 (2012).

[24] P. A. Sharma, J. S. Ahn, N. Hur, S. Park, S. B. Kim, S. Lee, J.-G. Park, S. Guha, S.-W. Cheong, “Thermal Conductivity of Geometrically Frustrated Ferroelectric YMnO3: Extraordinary Spin-Phonon Interactions”, Physical Review Letters vol. 93, 177202 (2004).